AIAA Aviation
22-26 June 2015, Dallas, TX
33rd AIAA Applied Aerodynamics Conference

Optimization of the Aerodynamic Performance of Regional and Wide-Body-Class Blended Wing-Body Aircraft

Thomas A. Reist* and David W. Zingg†
Institute for Aerospace Studies, University of Toronto
4925 Dufferin St., Toronto, Ontario, M3H 5T6, Canada

High-fidelity aerodynamic shape optimization based on the Reynolds-averaged Navier-Stokes equations is used to optimize the aerodynamic performance of conventional and blended wing-body (BWB) aircraft for both regional and wide-body aircraft segments. Trim-constrained drag-minimization is performed for both classes, with optimized conventional designs serving as a performance reference for the BWB concepts. It is found that a 'classically' shaped regional-class BWB yields no drag savings when compared to the conventional reference aircraft. An exploratory optimization with significant geometric freedom is then performed to explore the aerodynamic potential of small BWBs. This results in a novel shape with a slender lifting fuselage and distinct wings. Based on this exploratory result, a refined regional jet BWB is designed and optimized. With a span constrained by code 'C' gate limits and having the same wing-only span as the conventional reference aircraft, this new design produces 7% less drag than the reference aircraft and a 21% lift-to-drag benefit. The classical BWB configuration is found to be nearly aerodynamically optimal for wide-body-class BWBs. The wide-body BWB considered offers almost a 9% drag reduction and a 21% increase in the lift-to-drag ratio relative to the conventional aircraft.

I. Introduction

With increasing oil prices and concern about both the exhaustion of fossil fuels and their contribution to climate change, the need for more fuel efficient aircraft is becoming more pronounced for both economic and environmental reasons. Although there have been great advances in transport aircraft efficiency since the introduction of the de Havilland Comet in 1952, the conventional tube-and-wing (CTW) configuration remains to this day. Performance improvements have come from modifications to aerodynamic design, such as the use of supercritical airfoils, as well as high performance materials and increasingly fuel efficient engines. However a step change in fuel efficiency may be realized through novel configurations. One such configuration that has received much attention in recent years is the hybrid, or blended, wing-body (BWB). This design combines the aircraft fuselage and wings into one tightly integrated airframe with improved aerodynamic, structural, propulsive, and acoustic efficiency.

The BWB has the potential to be more aerodynamically efficient than conventional configurations for several reasons. For a given internal volume, the BWB has less wetted surface area, leading to a better lift-to-drag ratio.[1] It has also been shown to be more area-ruled than conventional designs, which allows for reduced wave drag and potentially higher cruise speeds.[1] The overall shape of the BWB is also cleaner than a conventional design, leading to reduced interference drag. Structurally, the aerodynamic lifting loads are more closely aligned with the weight of the aircraft due to the lifting fuselage, leading to reduced bending loads in the main wing structure and therefore lower structural weight.[1] The use of a well integrated propulsion system, such as boundary-layer-ingestion or distributed propulsion, can lead to propulsive efficiencies. A

*Ph.D. Candidate, AIAA Student member, tom.reist@utoronto.ca
†Professor and Director, J. Armand Bombardier Foundation Chair in Aerospace Flight, Associate Fellow AIAA, dwz@oddjob.utias.utoronto.ca

well integrated propulsion system on the top of the aircraft can also provide significant noise reductions due to the acoustic shielding provided by the aerodynamic surfaces.[2] The highly integrated nature of the design allows for efficiency improvements; however this also increases the design challenges stemming from such a highly coupled configuration.

One of the main structural challenges associated with the BWB is the lack of the efficient cylindrical pressure vessel present in conventional designs. Much work has been dedicated to the design of efficient composite structures tailored for handling these pressure loads.[3–5] Due to its tailless nature, stability and control can be challenging with this design. Work has been done on addressing some of these issues.[6,7] With such a radically different design, certification and customer acceptance must also be addressed. Finally, perhaps the biggest obstacle to the development of the BWB is the financial risk associated with pursuing such a novel design. However, as rising fuel prices continue to reduce operating profits, the potential benefits of this unconventional design may justify its development.

Several large projects around the world have focused on the development of the BWB design. In the United States, Boeing and NASA have been involved in the identification and development of enabling technologies required for the BWB design,[1,3,6,8–10] with contributions leading to the X-48 flight demonstrators. A BWB design focused on noise reduction has been developed as part of Cambridge and MIT's 'Silent' Aircraft Initiative.[2,11] In Europe, two of the main projects relating to BWB design are the Multidisciplinary Optimization of a Blended Wing Body (MOB)[12] and the Very Efficient Large Aircraft (VELA)[13] projects.

Aerodynamic shape optimization has been applied to the BWB design at a variety of fidelity levels. Peigin and Epstein[14] used a Navier-Stokes solver and genetic optimizer for the optimization of the MOB configuration for multiple operating points with airfoil, dihedral and twist design variables. Qin et al.[15] performed spanload optimization through twist modification as well as 3D surface optimization using both Euler and Navier-Stokes solvers. Both airfoil and sweep optimization were performed by Le Moigne and Qin[16] using a discrete adjoint method with an Euler solver. They demonstrated that the imposition of pitching moment constraints has a large impact on the optimal shape, yet only a small performance penalty must be paid. The performance improvements obtained using Euler-based optimization are also realized when evaluated with a Reynolds-averaged Navier-Stokes (RANS) solver. The challenge of considering stability and control of flying-wings during aerodynamic shape optimization has been addressed by Mader and Martins[17] through the application of a time-spectral method for optimizing in the presence of static and dynamic stability constraints. A small BWB was optimized by Kuntawala et al.[18] using a large number of geometric design variables for full 3D surface optimization. More recently, Lyu and Martins optimized an 800 passenger BWB using both the Euler[19] and RANS[20] equations subject to trim, static-stability, and root bending-moment constraints. Previous work by the present authors includes single and multipoint optimization of a regional-class BWB using both the Euler and RANS equations.[21] The impact of trim and stability constraints on the optimal BWB design at both on- and off-design conditions was examined. It was demonstrated that, for cruise, these constraints lead to a small performance penalty at on-design conditions through tailoring of the aerodynamic shape and aircraft weight distribution, while performance degrades significantly at off-design conditions. It was also shown, as with the work of Osusky and Zingg,[22] the necessity of using the RANS equations for aerodynamic design in order to not only capture the viscous components of drag, but also to properly determine and control the true local flow behaviour.

Historically, the focus of BWB design investigations has been on large capacity aircraft in the 400-1000 passenger range. The BWB's intrinsic design features lend themselves well to large aircraft. However this design may also offer advantages in the regional jet segment. Nickol examined a series of BWB aircraft ranging from 98-400 passengers.[9] As expected, the fuel burn benefit was most significant for the larger aircraft, with the 98 passenger aircraft burning more fuel than a comparable tube-and-wing aircraft. However, the fuel burn disadvantage of the small BWB was highly sensitive to drag. Thus, if a suitable drag reduction can be achieved through aerodynamic shape optimization, the BWB could potentially be more fuel efficient than the tube-and-wing aircraft for a variety of aircraft classes. The objective of this paper is to use high-fidelity aerodynamic shape optimization to evaluate the aerodynamic performance of BWB aircraft against equivalent conventional tube-and-wing designs for both regional and wide-body classes, thus helping to characterize the influence of BWB size on its relative aerodynamic efficiency.

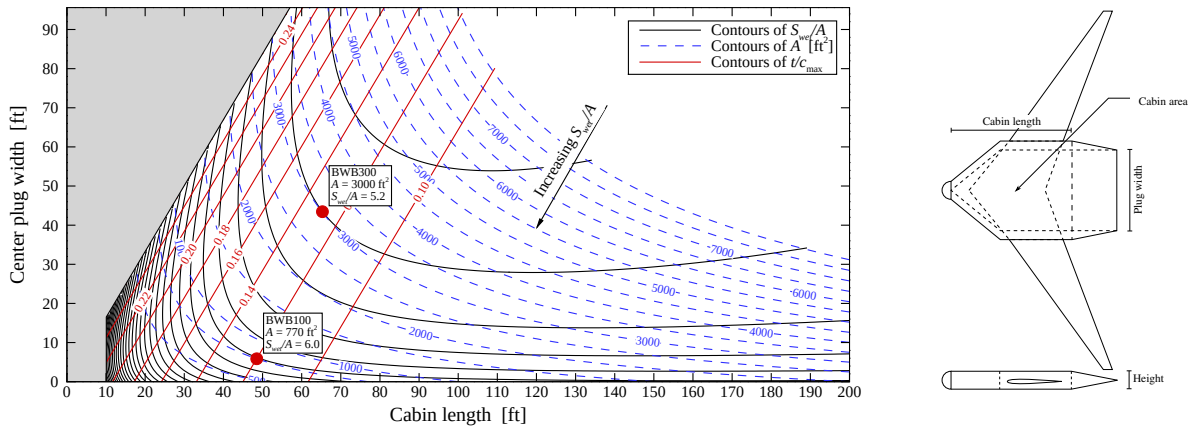

Figure 2: Wetted area per unit floor area, $S_{\mathbf{wet}}/A$, for a parametric BWB with a fuselage height of 10 ft, where A is the cabin floor area and $S_{\mathbf{wet}}$ is the wetted area. The parametric BWB model is shown on the right.

II. A Simple Geometric Analysis of BWB Scaling

One of the oft-quoted benefits of the BWB concept is its lower wetted area than comparable conventional tube-and-wing designs. To investigate how this wetted area benefit scales with aircraft size and shape, a simple geometric model for BWBs is constructed, from which the wetted area can be approximated in order to understand its correlation with aircraft size and shape.

This model consists of a conventional cylindrical fuselage of a given cabin length and height, with the nose and tail cone modelled as a semi-sphere and cone, respectively. This can be converted to a BWB by 'exploding' the cylinder laterally and adding a home plate shaped center plug in the cabin with the leading edge being a half cylinder and a wedge aft of the cabin. This model is shown in Figure 2. For a zero width center plug this model reduces to a cylindrical fuselage. For a given fuselage height, the length of the aft tail-wedge is determined by assuming a slope of the upper and lower surfaces of 15%, similar to existing transonic airfoils. For a given cabin length, height, center plug width, sweep angle (50°), and tail cone slope (15%) the fuselage geometry is fully defined, and the cabin floor area and the fuselage wetted area can be calculated. In addition, the 'masking' of wing area by the fuselage is accounted for. For a number of existing aircraft ranging from regional jets to large wide-bodies, correlations are made for wing span, b, and area, S, as a function of cabin floor area, A. These are found to be approximately $b = 2.062A^{0.574}$ and $S = 0.712A^{1.089}$, respectively, for A in square feet. Assuming a taper ratio of 0.1 allows for the determination of the size of a trapezoidal wing, also shown in Figure 2. The portion of the wing covered by the fuselage does not contribute to the wetted area.

First, this model is used to determine the wetted area per unit cabin floor area, S_{wet}/A, of conventional designs, i.e. with zero center plug width. For a 100-passenger design the floor area requirement is approximately 770 ft^2 and has a height of 10 ft; this yields $S_{\text{wet}}/A = 6.2$. A 300-passenger design requires a cabin floor area of approximately 3,000 ft^2 and has a height of 20 ft, resulting in $S_{\text{wet}}/A = 6.5$.

A model of S_{wet}/A for BWBs is now created. A center plug is added to a 10 ft height design, with the resulting contours of S_{wet}/A shown in Figure 2. This model reveals two important ideas: 1) The shape for a small BWB which minimizes S_{wet}/A, marked as BWB100 in Figure 2 and shown in Figure 1, has a slender fuselage with only a narrow center plug while, the optimal large BWB has a wide body as indicated in Figure 2 and shown in Figure 1. 2) The S_{wet}/A for the small BWB is only 3% lower than the similarly sized conventional tube-and-wing, while for the large BWB this benefit is 20%.

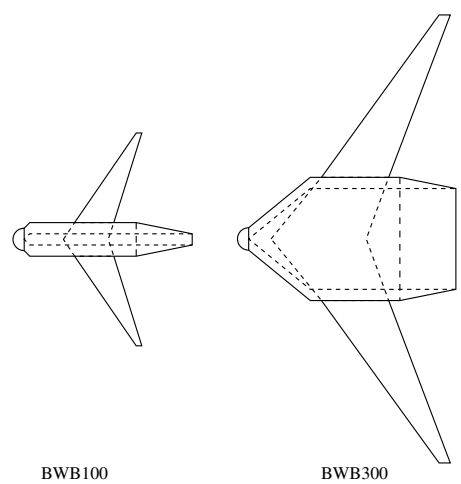

Figure 1: The BWB shapes for minimum $S_{\mathbf{wet}}/A$ for 100 and 300-passenger BWBs as predicted by the model in Figure 2.

While this 10 ft diameter does provide sufficient underfloor

cargo volume, the cargo compartment height is approximately 2 ft which would preclude the use of existing unit load devices (ULDs) and present operational challenges, particularly for larger aircraft. Should a larger height of 15 ft be used to accommodate LD3s, the same trends still hold; however the minimum S_{wet}/A shape is longer with a smaller plug width, and the magnitude of S_{wet}/A for a given floor area is increased. This 15 ft height would not be practical for the 100-passenger design, as the fuselage would reduce to a conventional cylinder and become very short. However, for the 300-passenger design, this larger diameter would likely be required in order to house the ULDs, in which case S_{wet}/A increases from 5.2 to 5.8, still 11% lower than the conventional reference.

This is a very simple analysis which neglects many considerations and simply tries to minimize wetted area. High-fidelity analysis and optimization of both regional and wide-body-class aircraft is presented in the following sections to more accurately establish the aerodynamic performance of BWB aircraft as a function of size and shape.

III. Design Problem

Conventional tube-and-wing (CTW) and BWB configurations are considered in this work, where the CTW designs serve as a performance reference for the BWB designs. Both regional jet (RJ) and wide-body class aircraft are considered. The RJ has a single-class capacity of 100 passengers, with a maximum range capability of 2,000 nmi plus reserves. This is similar to the design mission of the Embraer E190. The wide-body aircraft has a two-class capacity of 300 passengers, with a maximum range of 9,500 nmi plus reserves. This is similar to the Boeing 777-200LR. The nominal missions to be optimized are, for the RJ, a single-stage 500 nmi mission at 36,000 ft and Mach 0.78, and for the wide-body, a 6,000 nmi mission with an initial cruise altitude of 32,000 ft at Mach 0.84.

Both the CTW and BWB baseline designs are developed using a low-fidelity tool that incorporates aerodynamic and weight-and-balance analyses using the methods of Roskam,[23] Torenbeek,[24] and Raymer.[25] For the BWB designs, the weight of the center-body structure is obtained using the method of Bradley.[26] The remaining structure, systems, fuel, and operational item weights of the BWBs are assumed to be similar to those of CTW aircraft. The same low-fidelity aerodynamic models are used for both aircraft, with the BWB being treated simply as a wing. Details of each design are presented below, with all estimates based on current technology levels. This weight estimation methodology has been evaluated for a series of CTW designs against publicly available data, and for BWB aircraft against the results of Nickol.[9] The methods used to choose the mission profiles and to develop the baseline designs are very low-fidelity and do not represent full system-optimal design or operation. Instead, they are meant only to serve as a reasonable starting point for the high-fidelity optimization.[a]

A. Baseline Conventional Tube-and-Wing Designs

The baseline CTW designs, referred to as CTW100-0 and CTW300-10 for the RJ and wide-body respectively, are modeled after the Embraer E190 and Boeing 777-200LR using publicly available data.[27,28] Estimates for aircraft weight and performance are obtained via the methods described above. The low-fidelity models of the baseline RJ design and wide-body are shown in Figures 3 and 4, respectively. Design information for both the RJ and wide-body is given in Tables 1 and 2, respectively.

B. Baseline Blended Wing-Body Designs

The baseline BWB designs, referred to as BWB100-02 and BWB300-00 for the RJ and wide-body respectively, resemble a 'classic' BWB shape, i.e. similar to a scaled-down version of Liebeck's[1] designs. For the RJ, the span is chosen to be 118 ft to comply with ICAO code 'C' gate requirements while the wide-body span is 213 ft in order to be the same as the CTW reference aircraft. For the RJ BWB, cargo is housed outboard of the cabin, while for the wide-body BWB, cargo is held beneath the cabin. The low-fidelity model is shown in Figure 5 for the RJ, and in Figure 6 for the wide-body. The corresponding design information is shown in Tables 3 and 4, respectively.

[a] While there is uncertainty in the weight estimates, particularly for the BWBs, it should be noted that the BWB weights relative to the CTWs are similar to those of Nickol, i.e. both Nickol's BWBs and those presented here are heavier than their CTW equivalents. An absolute value comparison is not possible due to Nickol's use of advanced technologies not considered here.

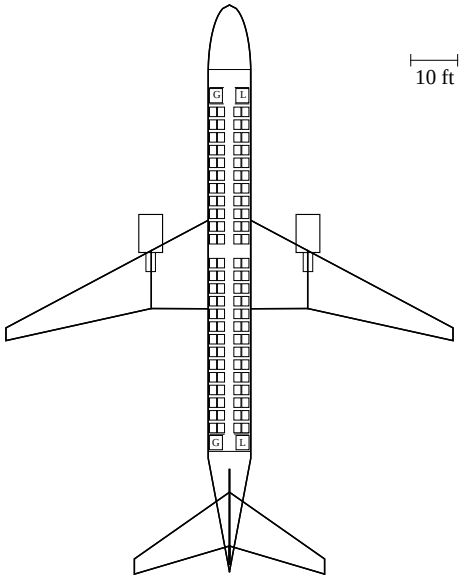

Figure 3: Baseline CTW100-10 geometry.

Capacity		
Passengers + crew	100+5	
Max payload	28,400	lb
Geometry		
Reference area	1,000	ft^2
Total span	94	ft
Length	119	ft
MAC	13.1	ft
Aspect ratio	8.8	
Weight		
MTOW	107,700	lb
OEW	58,800	lb
Wing load at MTOW	108	lb/ft^2
Nominal mission cruise		
Range	500	nmi
Altitude	36,000	ft
Mach number	0.78	
Reynolds number	23	$\times 10^6$
Weight*	92,900	lb
C_L*	0.46	
CG location*	55	ft

* At start of cruise

Table 1: Baseline CTW100-10 design summary.

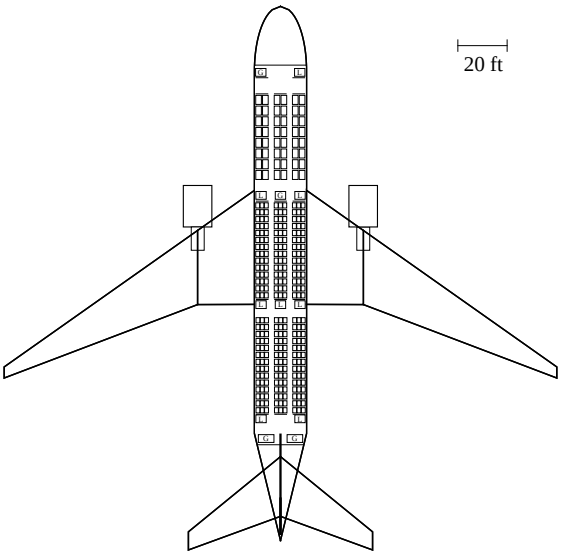

Figure 4: Baseline CTW300-10 geometry.

Capacity		
Passengers + crew	300+10	
Max payload	141,000	lb
Geometry		
Reference area	4,990	ft^2
Total span	213	ft
Length	206	ft
MAC	30.3	ft
Aspect ratio	9.1	
Weight		
MTOW	775,500	lb
OEW	330,900	lb
Wing load at MTOW	155	lb/ft^2
Nominal mission cruise		
Range	6,000	nmi
Altitude	32,000	ft
Mach number	0.84	
Reynolds number	68	$\times 10^6$
Weight*	625,000	lb
C_L*	0.44	
CG location*	97	ft

* At start of cruise

Table 2: Baseline CTW300-10 design summary.

The assumption is made that the BWB designs will require some form of lateral stabilizer. It is assumed that two vertical stabilizers outboard of the engines will be used so as to provide noise shielding. These stabilizers are sized such that they have sufficient area to counteract a one-engine-inoperative yawing moment, given the same fin lift coefficient as the baseline conventional aircraft.

From the basic geometric information provided by the low-fidelity design, full 3D surface models are created using the geometry toolbox developed by Gagnon and Zingg[29] and are shown in Figure 7. The

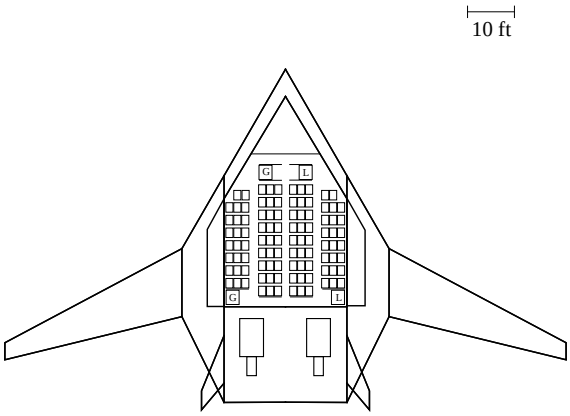

Figure 5: Baseline BWB100-02 geometry.

Capacity		
Passengers + crew	100+5	
Max payload	28,400	lb
Geometry		
Reference area	2,734	ft^2
Total span	118	ft
Length	70	ft
MAC	42.4	ft
Aspect ratio	5.1	
Weight		
MTOW	119,700	lb
OEW	69,800	lb
Wing load at MTOW	43.8	lb/ft^2
Nominal mission cruise		
Range	500	nmi
Altitude	36,000	ft
Mach number	0.78	
Reynolds number	76	$\times 10^6$
Weight*	104,600	lb
C_L*	0.19	
CG location*	41	ft

* At start of cruise

Table 3: Baseline BWB100-02 design summary.

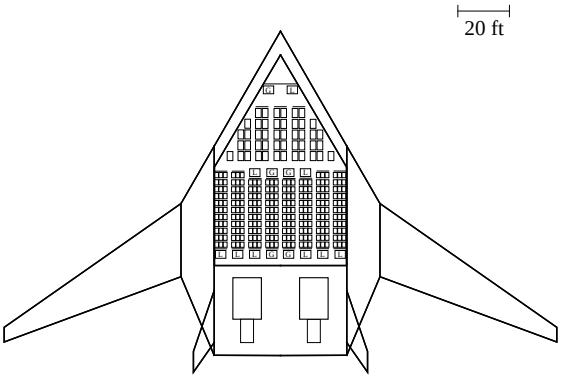

Figure 6: Baseline BWB300-00 geometry.

Capacity		
Passengers + crew	300+10	
Max payload	141,000	lb
Geometry		
Reference area	8,955	ft^2
Total span	213	ft
Length	90	ft
MAC	75.4	ft
Aspect ratio	5.1	
Weight		
MTOW	768,500	lb
OEW	350,200	lb
Wing load at MTOW	85.8	lb/ft^2
Nominal mission cruise		
Range	6,000	nmi
Altitude	32,000	ft
Mach number	0.84	
Reynolds number	169	$\times 10^6$
Weight*	622,300	lb
C_L*	0.24	
CG location*	76	ft

* At start of cruise

Table 4: Baseline BWB300-00 design summary.

baseline CTW wing is untwisted and uses the SC(2)-0012 section at the root and SC(2)-0010 at the tip. The baseline BWB body uses SC(2)-0014 sections, with SC(2)-0012 and SC(2)-0010 sections at the wing root and tip, respectively. These models do not include any vertical stabilizers in order to simplify grid generation and because their size and shape are determined by flight conditions that are not considered here.

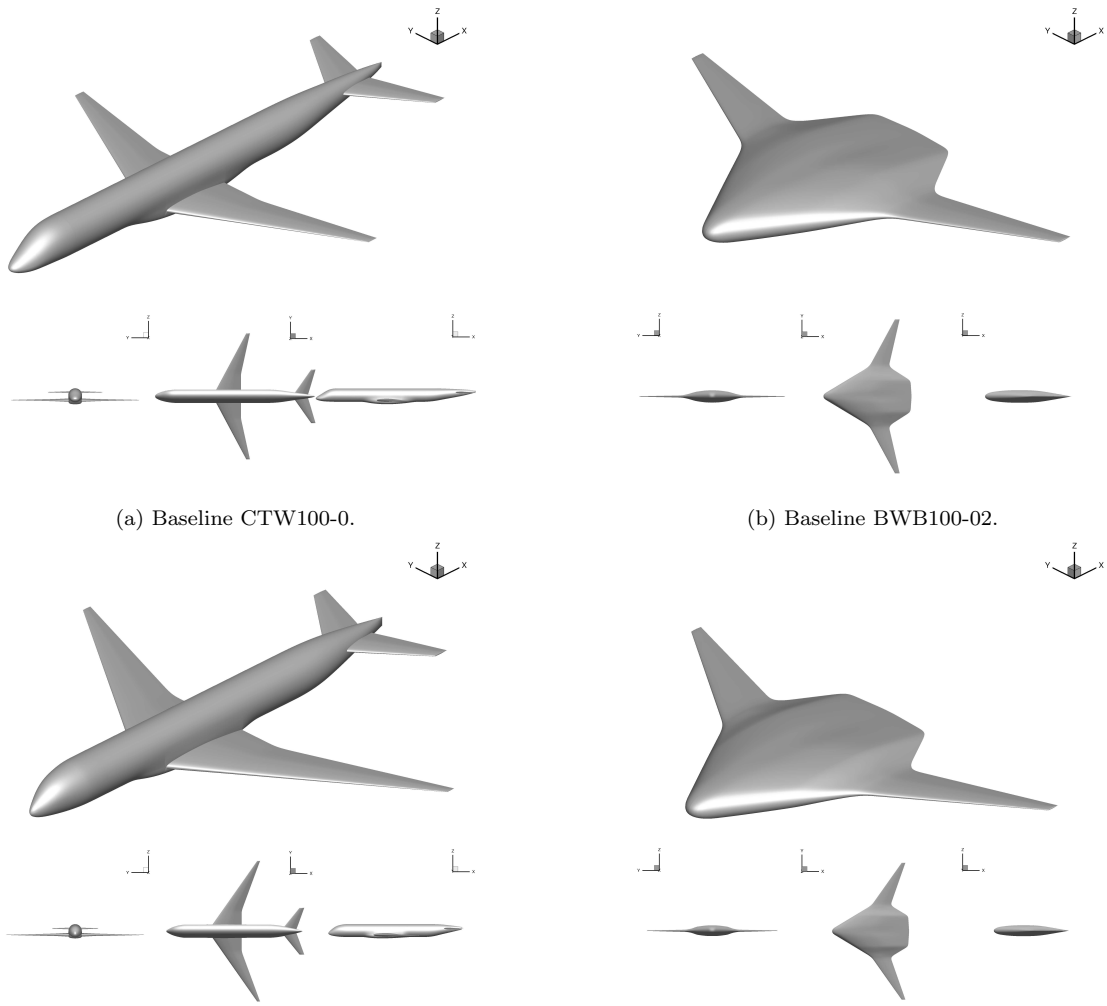

(a) Baseline CTW100-0.

(b) Baseline BWB100-02.

(c) Baseline CTW300-10.

(d) Baseline BWB300-00.

Figure 7: Full 3D models of the CTW and BWB baseline designs. (RJ and wide-body designs not shown to the same scale.)

IV. Aerodynamic Shape Optimization

A. Aerodynamic Shape Optimization Framework

The aerodynamic shape optimization (ASO) algorithm used comprises three main components: 1) a multi-block Newton-Krylov-Schur solver for the Euler[30] and RANS equations with the one-equation Spalart-Allmaras turbulence model,[31] 2) a B-spline geometry parameterization which is coupled with an integrated linear elasticity mesh movement strategy,[32] and 3) the gradient-based optimizer SNOPT[33] with gradients calculated using the discrete adjoint method.[32,34]

The flow solver is a multiblock finite-difference parallel implicit solver that uses summation-by-parts operators for spatial discretization and simultaneous approximation terms for the imposition of boundary conditions and block interface conditions. The Krylov subspace method Generalized Minimum Residual (GMRES) is used with approximate Schur preconditioning in an inexact Newton method for the solution of the discrete equations. Details of the flow solver can be found in Hicken and Zingg[30] and Osusky and Zingg.[31]

At each optimization iteration for which a geometric shape change occurs, the computational grid must be moved to reflect this change. To accomplish this, each block of the computational grid is fitted with a B-spline volume. The design variables for the optimization can be either the B-spline control points on

the aerodynamic surface, or the B-spline parameterization can be embedded within a free-form deformation volume that can be controlled through 'axial curves', as described by Gagnon and Zingg.[35] For this work direct control of the B-spline control points is used. As the B-spline control points on the aerodynamic surface are moved, each B-spline volume block is treated as a linear elastic solid, for which a finite-element solution is obtained to define the new shape of the B-spline volume. The computational grid is then recovered from this new B-spline volume. This method has been found to be very robust for large shape changes while being relatively inexpensive. Details can be found in Hicken and Zingg.[32]

Due to the high cost of evaluating the flow equations, a gradient-based optimizer is used for optimization, as gradient-based optimizers typically require fewer function evaluations than genetic algorithms.[36] The penalty paid is that for multimodal optimization problems only a local optimum may be found. This can be addressed using the gradient-based global optimization techniques proposed by Chernukhin and Zingg.[37] However, such an approach is not used here. The gradients of the objective and constraints are evaluated using the discrete adjoint method. This method is advantageous for problems with many design variables, as the cost of the gradient evaluation is nearly independent of the number of design variables. The number of adjoint solutions required is proportional to the number of objectives and constraints which depend on the flow properties. Since this can require significant computational cost for practical problems, an efficient method of solving the linear system of the adjoint problem is required. For this, a modified, flexible version of the Generalized Conjugate Residual with Orthogonalization and Truncation (GCROT) algorithm is used.[38] The gradient-based optimizer SNOPT is used, as it allows for the solution of large-scale constrained problems. Details of the adjoint method and its integration with the flow solver and mesh movement are given by Hicken and Zingg,[32] while the details of SNOPT are described by Gill et al.[33]

The above algorithm has been used extensively for ASO of various problems including induced drag minimization of non-planar wings,[39] optimization of wings in transonic[40] and turbulent flows,[34] the design of low-sweep wings,[41] investigation of the multimodality of ASO problems,[37] and the optimization of unconventional[29,42] and BWB[18,21] aircraft. This framework has also been extended to aerostructural optimization.[43,44]

B. Optimization Definition

All designs are optimized at a condition that corresponds to the start of the cruise segment of the nominal mission. The operating conditions for each design are shown in the previous section.

The surface CFD grid and the geometry parameterization are shown in Figure 8. The background surface shows the CFD grid, while the foreground surface shows the B-spline control grid, and the locations of the different geometric design variables are indicated. The design variable definition is that described in Osusky et al.[34] A portion of the BWB body upper surface is cut away to show the cabin shape. The angle-of-attack is a design variable for both configurations and is limited to $\pm 3°$ due to deck angle requirements. The incidence angle of the CTW wing and tail are free to vary between $\pm 5°$. For the CTWs, the wing chord and twist are allowed to vary at the crank and tip, with linear variation between. For the BWBs, the chord and twist are variable at the centerline, outboard edge of the cabin, wing root, and tip, with linear variation between. The CTWs and BWBs have section control at 12 and 18 span-stations respectively, at each of which there are 22 section variables, 11 for each of the lower and upper surfaces. For each pair of lower and upper surface section shape variables there is a corresponding thickness constraint to prevent the thickness decreasing by more than 25% of the initial value. For the CTWs, geometric changes to the fuselage caused by changes of the wing/tail root are handled via the method described in Osusky et al.[34] The CTW wing is divided into two segments, one inboard and one outboard of the crank. The BWB consists of three segments, one over the cabin, one transition segment between the edge of the cabin and the wing root, and one for the wing. The span of each of these segments can vary, but the total span remains fixed. The quarter-chord sweep of the CTW wing and the BWB wing is fixed. The sweep of the transition region of the BWB, between the cabin and the wing, is free to vary such that the optimizer can position the wing to minimize trim drag. The volume of both the CTW and BWB wings is constrained such that sufficient volume exists in the wing for fuel (4,500 gal for the RJ and 48,000 gal for the wide-body), where 80% of the outer mold line volume is usable. The outer mold line of the BWB is constrained such that it does not violate the specified BWB cabin shape, shown for the RJ by the red polyhedron in Figure 8b. Lift is constrained to be equal to the weight at the start of cruise, and the pitching moment about the center of gravity must be zero. There are a total of 273 effective design variables for the CTWs, and 407 for the BWBs. The design variables and constraints are the same for both the RJ and wide-body optimization problems.

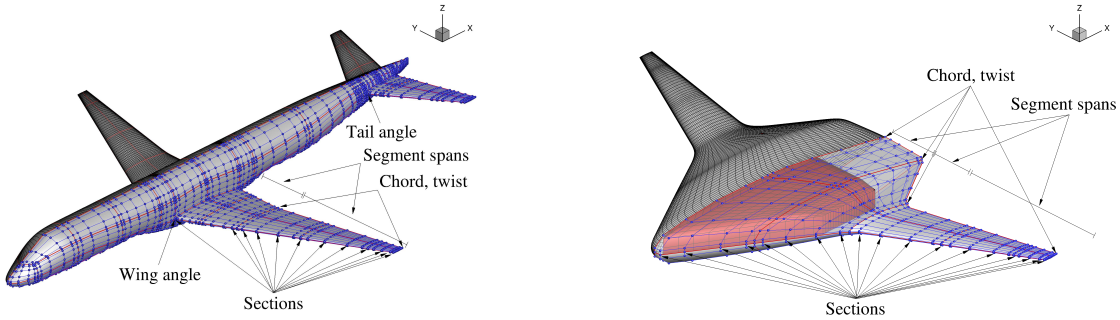

(a) CTW design variables.

(b) BWB design variables

Figure 8: Surface geometries for the CTW and BWB baselines showing both the surface CFD mesh and control mesh along with the types and locations of the geometric design variables. The upper surface of the BWB body is translucent to reveal the polyhedron that encloses the cabin. (Not shown to the same scale.)

For RANS-based optimization problems with free wing area it is critical that the ratio of induced and friction drag is predicted accurately such that the optimizer can properly trade friction drag for induced drag by changing the wing area. To ensure that the optimizations are being performed on a grid that accurately captures this friction-pressure drag relationship, a grid convergence study is performed for the RJ on both the baseline CTW and BWB. The resulting grid convergence plot for the BWB is shown in Figure 9 for grids ranging from 764,000 to 11×10^6 nodes. It is seen that the coarsest grid of 764,000 nodes does not capture the proper relationship between friction and pressure drag, while for grids of 1.5×10^6 nodes and larger the friction-pressure drag relationship is properly captured. Thus the 1.5×10^6 node grid, indicated in Figure 9, is used for optimizations. A similar study is performed to verify the grids used for the CTW optimizations which results in the use of a 6.3×10^6 node grid. Both of these grids have an off-wall spacing of $y^+ \approx 1.0$. While these grids are too coarse to provide accurate force and moment estimates, it has been found that they are capable of capturing the dominant flow features and thus properly designing the shape.

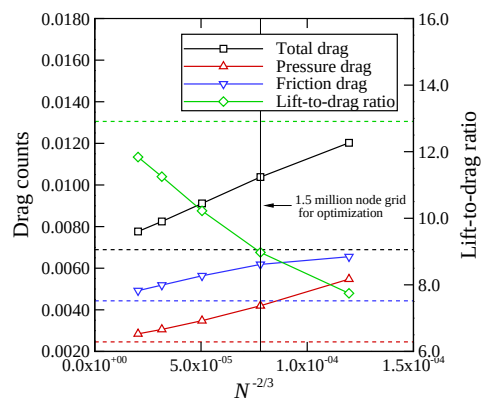

Figure 9: Grid refinement study at constant lift, for grids between 764,000 and 11×10^6 nodes. The dashed horizontal lines indicate the Richardson extrapolated values.

In order to determine the final force and moment coefficients of the optimized designs, grid convergence studies are performed for each optimized design. For each design a sequence of 4 grids with 1, 2, 4, and 8 times as many nodes as the optimization grid is created, and Richardson extrapolation is used with an assumed order of accuracy of 2 to determine the grid-converged performance estimates. All results presented in this paper are based on such grid convergence studies.

Since the vertical fins are not modelled in the high-fidelity CFD, their drag contribution is accounted for by calculating the friction drag coefficient of the CTW tail, scaling this by the fin area, and adding this to the drag predicted for the rest of the configuration by the high-fidelity CFD. All numbers quoted in this paper contain this drag contribution unless stated otherwise.

C. Optimization Results

Each optimization is run for between 100-200 design iterations at which point all constraints are satisfied and there is no longer improvement in the objective function between iterations. The resulting shapes are shown in Figure 10. For the CTW optimizations, the optimizer adds washout to reduce induced drag and modifies the sections to remove any shocks. The resulting designs are shock-free and nearly separation-free, where a small recirculation region is present at the trailing edge of the tail-body junction of both CTW designs. The wing area is decreased for both CTWs; by 6.5% for the RJ and 6.9% for the wide-body CTW.

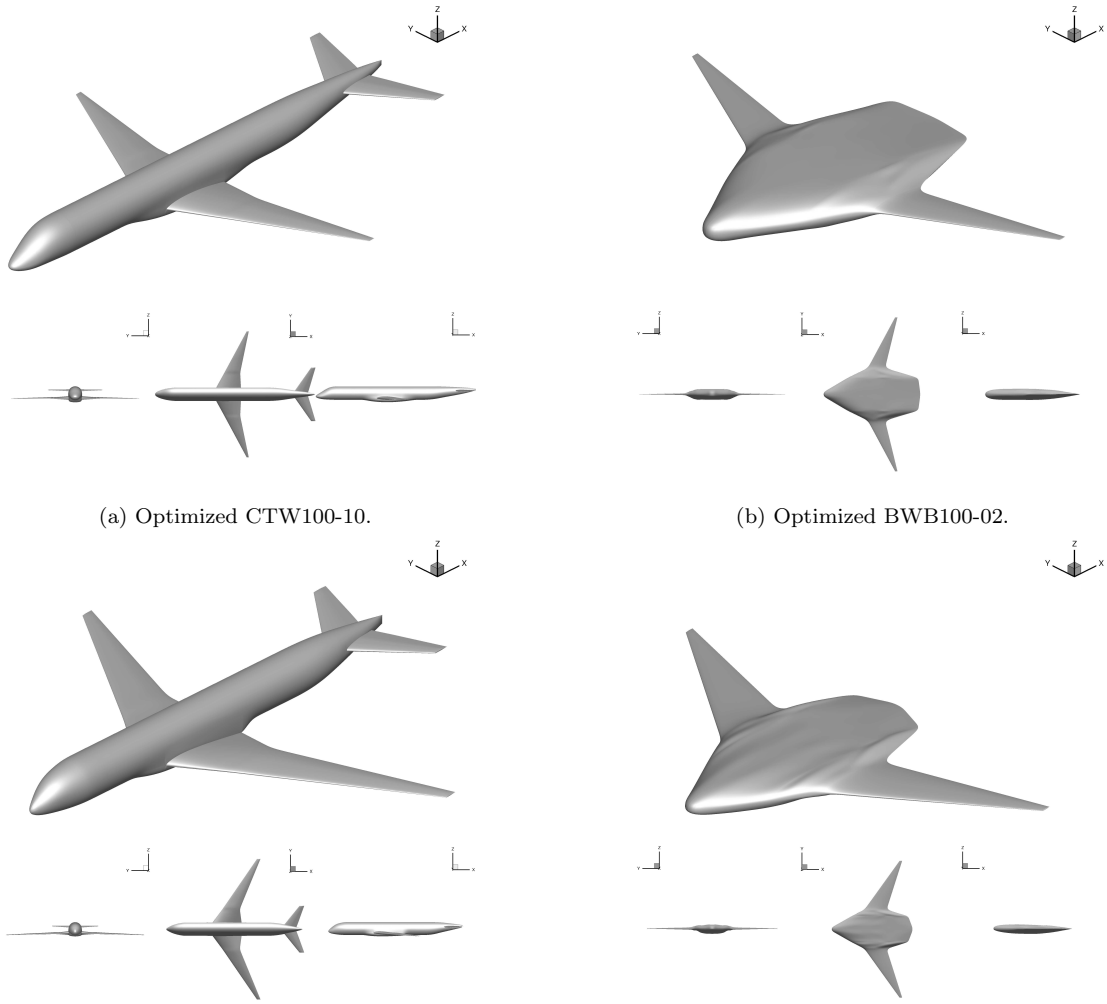

(a) Optimized CTW100-10.

(b) Optimized BWB100-02.

(c) Optimized CTW300-10.

(d) Optimized BWB300-00.

Figure 10: Optimized CTW and BWB designs.

For the BWBs, the action of the optimizer is to closely wrap the outer mold line of the body around the prescribed cabin shape to minimize wetted area while increasing the chord at the centerline to decrease the maximum t/c. Washout is added to the wing, and the sections along the span are shaped to eliminate shocks and remove separation. The body of the RJ carries 42% of the total lift, while that of the wide-body carries 32%.

The wide-body BWB offers a lift-to-drag benefit over its CTW counterpart of almost 7%, due in part to its 12% lower wetted area, as both designs have the same span. The RJ BWB has a lift-to-drag ratio 13% higher than the CTW reference aircraft. A significant lift-to-drag benefit is expected purely by the fact that the BWB has a 26% larger span, yet some of this advantage is negated by the fact that this concept has an 8% higher wetted area. This motivates the question of whether there is a different BWB configuration that is more beneficial for smaller aircraft sizes, which forms the basis for the following section.

V. Exploratory Aerodynamic Shape Optimization

To investigate alternative BWB shapes which may offer improved aerodynamic efficiency, a pair of exploratory optimizations is performed with significant geometric freedom for both a RJ and wide-body sized BWB. The starting shapes for the optimizations are the baseline BWBs, BWB100-02 and BWB300-00. Since large geometric changes are expected, which can have a large impact on the weight and therefore the required

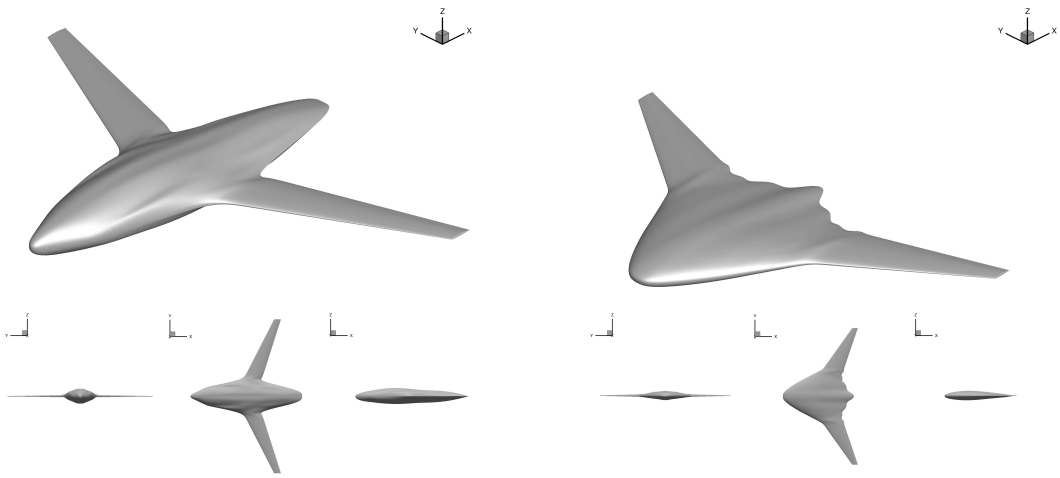

(a) Optimal RJ BWB shape.

(b) Optimal wide-body BWB shape.

Figure 11: Resulting shapes from the exploratory optimization. (Not shown to the same scale.)

lift, the optimization objective is to maximize the lift-to-drag ratio instead of minimize drag subject to a lift constraint. For the same reason, no pitching moment constraint is applied. The design variables and constraints for this problem are the same as for the BWB optimization presented in the previous section, with the notable exceptions that: 1) the BWB body is defined up to the wing root, i.e. there is no 'transition' joint, 2) the leading and trailing edges of the body are not required to be straight, and 3) the cabin shape constraint, which is highly restrictive, is replaced with body area and volume constraints. The cabin floor area and usable cabin volume of the CTW baselines are approximately 770 ft^2 and 5,000 ft^3 respectively for the RJ, and 3,000 ft^2 and 21,000 ft^3 respectively for the wide-body. The assumption is made that only 50% of the projected area and volume of the body is usable for housing the cabin due to minimum dimension requirements; the area and volume of the body are constrained accordingly. There are a total of 425 effective design variables for each case.

The optimizer removes all shocks from both designs and decreases the wetted area by 9.7% for the RJ and by 6.4% for the wide-body. This results in a lift-to-drag ratio of 26.4 for the RJ and of 27.1 for the wide-body; the drag contribution for the vertical fins is not added here. For both designs the projected area of the body, as well as the volumes of the body and wing go to their lower bounds. The resulting shapes are shown in Figure 11. For the RJ, the optimizer has decreased the body width, with an associated increase in the span of the wing, and increased the slenderness ratio of the body. The section at the centerline has a maximum t/c of 14%. Note the similarity of the shape in Figure 11a to that predicted for the 100-passenger BWB via the simple geometric analysis in Figure 1. For the wide-body, the wing area is increased, and the chord along the body is decreased, leading to almost a pure flying-wing shape. Note the exploitation by the optimizer of the ability to form a nonlinear trailing edge. The physical motivation for this feature is unclear. However it has been found that it only provides a very marginal aerodynamic benefit, and is possibly the result of numerical artifacts being exploited by the optimizer. In contrast to the RJ result, the wide-body maintains a broad body. This again is similar to the result seen in the geometric analysis of Section II. Several variations of this problem formulation have been investigated, including with various utilization factors for the body area/volume, and by using the same 3-segment span definition which was used for the trim-constrained problems. All of these variations lead to the similar conclusion that for RJ-class aircraft the aerodynamically optimal shape consists of a narrow body with a distinct wing, and for the wide-body-class the optimal shape resembles a pure flying-wing with a very span-loaded cabin.

Since this is a single-discipline optimization, any changes in structural weight caused by changes in span-loading of the payload, and by different cabin shapes are not captured; hence this optimization represents strictly an aerodynamically optimal design. A full aerostructural optimization would be required to capture this weight-drag trade-off in the exploratory optimization.

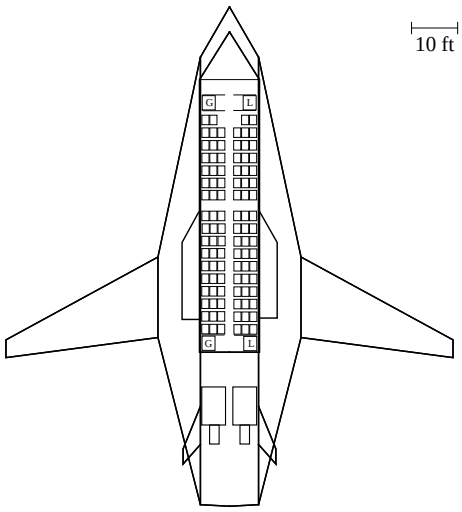

Figure 12: Refined BWB100-10 geometry.

Capacity		
Passengers + crew	100+5	
Max payload	28,400	lb
Geometry		
Reference area	2868	ft^2
Total span	94	ft
Length	105	ft
MAC	67.2	ft
Aspect ratio	3.1	
Weight		
MTOW	115,400	lb
OEW	65,000	lb
Wing load at MTOW	40.2	lb/ft^2
Nominal mission cruise		
Range	500	nmi
Altitude	36,000	ft
Mach number	0.78	
Reynolds number	121	$\times 10^6$
Weight*	100,000	lb
C_L*	0.17	
CG location*	54.2	ft

* At start of cruise

Table 5: Refined BWB100-10 design summary.

A. Refined Blended Wing-Body Design

While the exploratory result presented above has sufficient body volume and area to house the required cabin, it is not possible to fit a practical cabin shape within the resulting body shape due to minimum dimension requirements. Thus, the result of the exploratory optimization guides the design and optimization of refined BWB designs. Designs which imitate the results shown in Figure 11 are developed, and a cabin layout is designed which fits within the new shapes while maintaining straight walls and a practical seating configuration. In the case of the wide-body, this leads to a shape which is similar to the original baseline once these practical requirements are considered. Thus, it is determined that for the purposes of this work a refined wide-body BWB is not warranted. One possible refinement would be the relocation of cargo from under the cabin to outboard of the cabin. This shall be considered in future work. For the RJ BWB the overall shape is significantly different than that of the baseline; thus a refined design, referred to as BWB100-10, is created. This results in a 16-row, 3-3 cabin configuration, with baggage compartments outboard of the passenger cabin. While the span of the exploratory optimization was constrained to be 118 ft, the refined BWB uses a 94 ft span. This is because the narrower cabin of the refined BWB leads to less span-loading of the payload and thus a higher wing span for a given total span. The 94 ft span also allows a direct performance comparison with the baseline CTW. As with the baseline designs, a low-fidelity model of the refined BWB is created and shown in Figure 12, with the corresponding design information given in Table 5. Due to the small lateral offset of the engines and the long fuselage, the fins of this BWB are significantly smaller than those of the baseline.

A trim-constrained drag-minimization optimization of this refined RJ BWB design, the 3D model of which is shown in Figure 13, is performed in the same manner as the baseline BWB. The optimized design is shown in Figure 14. This optimized design has a wetted area of 5,922 ft^2, almost 6% lower than the optimized BWB100-02 design. The body carries 37% of the lift. The lift-to-drag ratio is 21.4, which is only 4.9% lower than the optimized BWB100-02, despite the fact that this design has a span of 94 ft.

Since both weight and aerodynamic performance are highly dependent on span, and a full aerostructural analysis is beyond the scope of this work, a study of the impact of span on performance is required. This is examined in the following section.

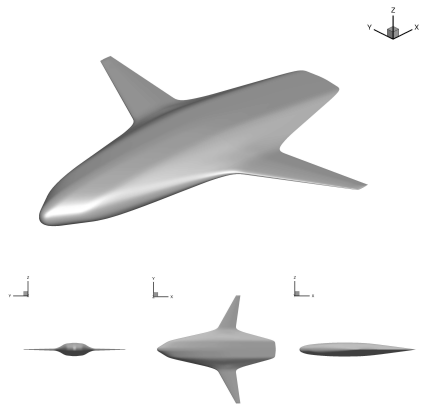

Figure 13: The refined BWB100-10 concept.

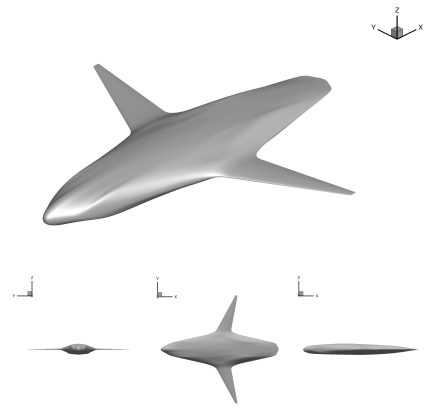

Figure 14: The optimized BWB100-10 concept.

	Design	Span [ft]	Bending span [ft]	Weight* [lb]	Area [ft^2]	Wetted area† [ft^2]	$L/D^{*\dagger}$ [–]	Relative drag [%]
RJ	CTW100-10	94	85	92,900	935	5,634	20.0	—
	BWB100-02	118	76	104,600	2,732	6,286	22.5	+0.1
	BWB100-03	130	88	107,700	2,813	6,444	23.3	−0.7
	BWB100-10	94	64	100,000	2,535	5,922	21.4	+0.4
	BWB100-12	118	88	105,000	2,674	6,189	24.3	−7.1
Wide-body	CTW300-10	213	193	624,900	4,757	22,279	24.2	—
	BWB300-00	213	136	622,300	8,581	19,585	25.8	−6.5
	BWB300-02	262	185	692,100	9,606	21,055	29.3	−8.6

* At start of nominal mission cruise

† Includes fin wetted area/drag contribution

Table 6: Design information for all optimized designs. Drag is given relative to the CTW reference aircraft for each class.

VI. Performance Comparison

For the CTW configuration a large body of prior art exists to aid in the determination of a system-optimal span. However for BWB concepts such prior art is not available. Thus, for each BWB design presented so far, a second set of designs is created with increased span to allow for the characterization of aerodynamic performance with span.

Here we introduce the concept of the 'bending span'. This is taken to be the portion of the total span which is subjected primarily to bending loads, and is defined as $b_{\text{bend}} = b - w_{\text{body}}$ where b is the total span, and w_{body} is the width of the fuselage/body. The span increases for the RJ BWBs are chosen such that they yield equivalent bending spans, and the bending span is similar to the RJ CTW design (85 ft). The span increase for the wide-body BWB is limited by the code 'F' gate limit. The bending span for each design is shown in Table 6. As with the baseline aircraft, low-fidelity models are created for each of these designs, the resulting weights of which at the start of cruise are shown in Table 6. In addition to the optimized designs already presented, each of these increased span derivatives is also optimized in the same manner. Note that the lift-to-drag values for the CTW aircraft are higher than typically seen for existing aircraft. This is due primarily to the fact that 1) this is a single-point, single-discipline optimization where drag has only been minimized at one operating condition and without any aerostructural considerations, and 2) nacelle and pylon drag, as well as excrescence and protuberance drag are not accounted for. These additional sources are not considered since there may be significant differences in the magnitude of these contributions between the two concepts, e.g. due to the use of pylon-mounted versus embedded engines for the BWB.

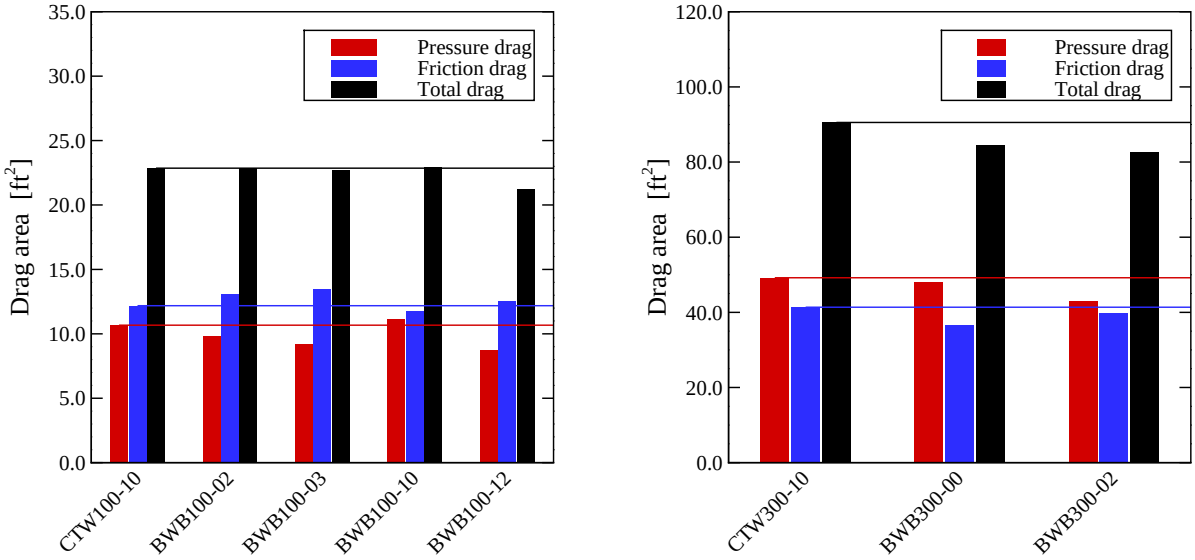

(a) RJ drag breakdown.

(b) Wide-body drag breakdown.

Figure 15: Breakdown of friction and pressure drag for each design. Given as drag area, D/q_∞, where D is the drag force and q_∞ is the free-stream dynamic pressure.

A. Regional Jet Performance

The original BWB100-02 span is increased to 130 ft; this design is referred to as BWB100-03 and has an 88 ft bending span. The BWB100-10 span is increased to 118 ft, for an 88 ft bending span, and is referred to as BWB100-12. The breakdown of friction and pressure drag for the RJ designs is shown in Figure 15a. The first BWB family, BWB100-0X, which has the classic BWB shape, gives higher friction drag than the reference aircraft due in part to its higher wetted area. Pressure drag, primarily composed of induced drag, is lower due to the higher span, but the higher weight of the BWBs negates much of this potential benefit. The total drag for the first family is thus similar to that of the conventional aircraft. The second family, BWB100-1X, based on the geometry shown in Figure 12, exhibits friction drag similar to the reference aircraft. The 94 ft span BWB100-10 has higher induced drag than the 94 ft span reference aircraft due to the higher weight, while the 118 ft span BWB100-12 shows an induced drag benefit from the higher span. The total drag of the 118 ft span BWB100-12 is 7.1% lower than the reference aircraft. Note that while this design has a 118 ft span, the bending span is roughly the same as the reference aircraft, i.e. to a first-order approximation, the drag reduction is achieved without an increase in wing weight relative to the CTW reference aircraft.

The lift-to-drag performance for every design is included in Table 6. The highest lift-to-drag ratio of 24.3 is obtained by the 118 ft span BWB100-12 design. This is 21.5% higher than the optimized reference conventional, CTW100-10. All of the BWBs offer a lift-to-drag benefit over the conventional design.

B. Wide-Body Performance

For the wide-body BWB, the BWB300-00 span is increased to 262 ft. This is limited by the gate constraint and leads to a bending span lower than that of the wide-body CTW; this design is referred to as BWB300-02. The breakdown of friction and pressure drag for the wide-body designs is shown in Figure 15b. Both of the BWB designs offer reduced friction drag due in part to their lower wetted area. The original span BWB, BWB300-00, has a small induced drag benefit due to its slightly lower weight. The increase in span for the BWB300-02 overcomes the corresponding weight increase to offer an induced drag benefit, such that this design is operating at a condition close to that for the maximum lift-to-drag ratio. The overall drag savings for the wide-body BWB is thus up to 8.6%. The low-fidelity model predicts a very large weight increase for the BWB when the span is increased to 262 ft. Whether such a weight increase is realistic is questionable, in which case the drag benefit for the larger span BWB may likely be higher. The large-span BWB, BWB300-02, offers a 21.1% lift-to-drag benefit over the conventional reference aircraft.

VII. Conclusions

The aerodynamic performance of both regional and wide-body-class BWBs was investigated and compared against equivalent conventional tube-and-wing designs. For regional-class BWBs it was found that 'classically' shaped BWBs do not offer a wetted area reduction, and their primary aerodynamic benefit is the ability to increase the span via span-loading of the payload. However the imposition of gate constraints can prevent the exploitation of this benefit, in which case the wetted area causes a prohibitive drag penalty. A novel regional jet BWB shape was found through high-fidelity RANS-based aerodynamic shape optimization and features a lifting fuselage with a distinct wing. This concept leads to lower wetted area than a classical BWB for regional-class aircraft. The extent of the span-loading of the payload is reduced compared to the classical shape; however it is still greater than for conventional tube-and-wing designs, thus allowing for a larger span for equivalent bending span. Using this new concept, a regional-class BWB was designed that provides a 7% drag reduction and a 21% higher lift-to-drag ratio compared to a similarly optimized conventional design. For wide-body-class aircraft the BWB concept does offer a wetted area reduction, and exploratory optimization confirmed that a classically shaped BWB is close to the aerodynamically optimal shape. Through both its wetted area reduction and the increased span enabled through span-loading, the wide-body BWB designs considered offer up to a 9% drag reduction and a 21% lift-to-drag ratio improvement relative to the equivalent conventional design.

Both regional and wide-body-class BWBs considered in this work offer significant aerodynamic efficiency improvements over conventional designs. However, higher weight compared to the conventional aircraft prevents much of this benefit from being realized in terms of a drag, and hence fuel-burn, reduction. Reducing empty weight, particularly for the regional-class BWBs will be essential in realizing this concept's full fuel-burn potential. More accurate weight estimation methodologies, particularly in the early design stages, will be required in order to determine with confidence the potential performance benefits of the BWB concept. Full aerostructural optimization can play an important role here, as the assumptions required in this paper could be eliminated and an aerostructurally optimal design could be found.

Future work will aim to investigate the potential benefits of this new regional jet BWB configuration in other flight conditions which are significant for this segment, such as climb and descent. The relative merits of these two concepts when operating conditions are allowed to vary will be considered. For the BWB designs, the impact of longitudinal static stability constraints on aerodynamic performance will also be considered.

Acknowledgments

Financial support is provided in part by the Natural Sciences and Engineering Research Council of Canada and the University of Toronto. Computations were performed on the General Purpose Cluster supercomputer at the SciNet HPC Consortium. SciNet is funded by: the Canada Foundation for Innovation under the auspices of Compute Canada; the Government of Ontario; Ontario Research Fund - Research Excellence; and the University of Toronto.

References

[1]Liebeck, R., "Design of the Blended Wing Body Subsonic Transport," *Journal of Aircraft*, Vol. 41, No. 1, 2004, pp. 10–25.

[2]Hileman, J. I., Spakovszky, Z. S., Drela, M., Sargeant, M. A., and Jones, A., "Airframe Design for Silent Fuel-Efficient Aircraft," *Journal of Aircraft*, Vol. 47, No. 3, 2010, pp. 956–969.

[3]Li, V. and Velicki, A., "Advanced PRSEUS Structural Concept Design and Optimization," *12th AIAA/ISSMO Multidisciplinary Analysis and Optimization Conference*, AIAA-2008-5840, Victoria, BC, September 2008.

[4]Mukhopadhyay, V., "Blended-Wing-Body Fuselage Structural Design for Weight Reduction," *46th Structures, Structural Dynamics and Materials Conference*, AIAA-2005-2349, Austin, TX, April 2005.

[5]Hansen, L. U., Heinze, W., and Horst, P., "Blended Wing Body Structures in Multidisciplinary Pre-Design," *Structural and Multidisciplinary Optimization*, Vol. 38, No. 1, 2008, pp. 93–106.

[6]Vicroy, D. D., "Blended-Wing-Body Low-Speed Flight Dynamics: Summary of Ground Tests and Sample Results," *47th AIAA Aerospace Sciences Meeting and Exhibit*, AIAA-2009-0933, Orlando, FL, January 2009.

[7]Voskuijl, M., La Rocca, G., and Dircken, F., "Controllability of Blended Wing Body Aircraft," *26th International Congress of the Aeronautical Sciences*, Anchorage, AL, September 2008.

[8]Gern, F. H., "Improved Aerodynamic Analysis for Hybrid Wing Body Conceptual Design Optimization," *50th AIAA Aerospace Sciences Meeting and Exhibit*, AIAA-2012-0249, Nashville, TN, January 2012.

[9]Nickol, C. L., "Hybrid Wing Body Configuration Scaling Study," *50th AIAA Aerospace Sciences Meeting and Exhibit*, AIAA-2012-0337, Nashville, TN, January 2012.

[10]Wakayama, S., "Blended-Wing-Body Optimization Problem Setup," *8th AIAA/USAF/NASA/ISSMO Symposium on Multidisciplinary Analysis and Optimization*, AIAA-2000-4740, Long Beach, CA, September 2000.

[11]Hileman, J. I., Spakovszky, Z. S., Drela, M., and Sargeant, M. A., "Airframe Design for "Silent Aircraft"," *45th AIAA Aerospace Sciences Meeting and Exhibit*, AIAA-2007-0453, Reno, NV, January 2007.

[12]Morris, A. J., "MOB: A European Distributed Multi-Disciplinary Design and Optimisation Project," *9th AIAA/ISSMO Symposium on Multidisciplinary Analysis and Optimization*, AIAA-2002-5444, Atlanta, GA, September 2002.

[13]Méheut, M., Grenon, R., Carrier, G., Defos, M., and Duffau, M., "Aerodynamic Design of Transonic Flying Wing Configurations," *CEAS Katnet II Conference on Key Aerodynamic Technologies*, Breme, Germany, May 2009.

[14]Peigin, S. and Epstein, B., "Computational Fluid Dynamics Driven Optimization of Blended Wing Body Aircraft," *AIAA Journal*, Vol. 44, No. 11, 2006, pp. 2736–2745.

[15]Qin, N., Vavalle, A., Le Moigne, A., Laban, M., Hackett, K., and Weinerfelt, P., "Aerodynamic Considerations of Blended Wing Body Aircraft," *Progress in Aerospace Sciences*, Vol. 40, No. 6, 2004, pp. 321–343.

[16]Le Moigne, A. and Qin, N., "Aerofoil Profile and Sweep Optimisation for a Blended Wing-Body Aircraft Using A Discrete Adjoint Method," *The Aeronautical Journal*, Vol. 110, No. 1111, 2006, pp. 589–604.

[17]Mader, C. A. and Martins, J. R. R. A., "Stability-Constrained Aerodynamic Shape Optimization of Flying Wings," *Journal of Aircraft*, Vol. 50, No. 5, 2013, pp. 1431–1449.

[18]Kuntawala, N. B., Hicken, J. E., and Zingg, D. W., "Preliminary Aerodynamic Shape Optimization Of A Blended-Wing-Body Aircraft Configuration," *49th AIAA Aerospace Sciences Meeting*, AIAA-2011-0642, Orlando, FL, January 2011.

[19]Lyu, Z. and Martins, J. R. R. A., "Aerodynamic Shape Optimization of a Blended-Wing-Body Aircraft," *51st AIAA Aerospace Sciences Meeting*, AIAA-2013-0283, Grapevine, TX, January 2013.

[20]Lyu, Z. and Martins, J. R. R. A., "Aerodynamic Shape Optimization Studies of a Blended-Wing-Body Aircraft," *Journal of Aircraft*, Vol. 51, No. 5, 2014, pp. 1604–1617.

[21]Reist, T. A. and Zingg, D. W., "Aerodynamic Shape Optimization of a Blended-Wing-Body Regional Transport for a Short Range Mission," *31st AIAA Applied Aerodynamics Conference*, AIAA-2013-2414, San Diego, CA, June 2013.

[22]Osusky, L. and Zingg, D. W., "Application of an Efficient Newton-Krylov Algorithm for Aerodynamic Shape Optimization Based on the Reynolds-Averaged Navier-Stokes Equations," *21st AIAA Computational Fluid Dynamics Conference*, AIAA-2013-2584, San Diego, CA, June 2013.

[23]Roskam, J., *Airplane Design Part V: Component Weight Estimation*, Aviation and Engineering Corporation, 1989.

[24]Torenbeek, E., *Synthesis of Subsonic Airplane Design*, Delft University, 1976.

[25]Raymer, D. P., *Aircraft Design: A Conceptual Approach*, American Institute of Aeronautics and Astronautics, 5th ed., 2012.

[26]Bradley, K. R., "A Sizing Methodology for the Conceptual Design of Blended-Wing-Body Transports," Tech. Rep. NASA/CR-2004-213016, NASA/Langley Research Center: Joint Institute for Advancement of Flight Sciences, 2004.

[27]Embraer Commercial Aircraft, *Embraer 190 Airport Planning Manual*, 2005, (Revision 10 - 18 February 2013).

[28]Boeing Commercial Airplanes, *777-200LR/-300ER/-Freighter Airplane Characteristics for Airport Planning*, 2009.

[29]Gagnon, H. and Zingg, D. W., "Geometry Generation of Complex Unconventional Aircraft with Application to High-Fidelity Aerodynamic Shape Optimization," *21st AIAA Computational Fluid Dynamics Conference*, AIAA-2013-2850, San Diego, CA, June 2013.

[30]Hicken, J. E. and Zingg, D. W., "A Parallel Newton-Krylov Solver for the Euler Equations Discretized Using Simultaneous Approximation Terms," *AIAA Journal*, Vol. 46, No. 11, 2008, pp. 2773–2786.

[31]Osusky, M. and Zingg, D. W., "A Parallel Newton-Krylov-Schur Flow Solver for the Navier-Stokes Equations Discretized Using Summation-By-Parts Operators," *AIAA Journal*, Vol. 51, No. 12, 2013, pp. 2833–2851.

[32]Hicken, J. E. and Zingg, D. W., "Aerodynamic Optimization Algorithm with Integrated Geometry Parameterization and Mesh Movement," *AIAA Journal*, Vol. 48, No. 2, 2010, pp. 401–413.

[33]Gill, P. E., Murray, W., and Saunders, M. A., "SNOPT: An SQP Algorithm for Large-Scale Constrained Optimization," *Society for Industrial Applied Mathematics Review*, Vol. 47, No. 1, 2005, pp. 99–131.

[34]Osusky, L., Buckley, H., Reist, T., and Zingg, D. W., "Drag Minimization Based on the Navier-Stokes Equations Using a Newton-Krylov Approach," *AIAA Journal*, Vol. 53, No. 6, 2015, pp. 1555–1577.

[35]Gagnon, H. and Zingg, D. W., "Two-Level Free-Form and Axial Deformation for Exploratory Aerodynamic Shape Optimization," *AIAA Journal*, 2015, (In press).

[36]Zingg, D. W., Nemec, M., and Pulliam, T. H., "A Comparative Evaluation of Genetic and Gradient-Based Algorithms Applied to Aerodynamic Optimization," *European Journal of Computational Mechanics*, Vol. 17, No. 1, 2008, pp. 103–126.

[37]Chernukhin, O. and Zingg, D. W., "Multimodality and Global Optimization in Aerodynamic Design," *AIAA Journal*, Vol. 51, No. 6, 2013, pp. 1342–1354.

[38]Hicken, J. E. and Zingg, D. W., "A Simplified and Flexible Variant of GCROT for Solving Nonsymmetric Linear Systems," *SIAM Journal of Scientific Computing*, Vol. 32, No. 3, 2010, pp. 1672–1694.

[39]Hicken, J. E. and Zingg, D. W., "Induced Drag Minimization of Nonplanar Geometries Based on the Euler Equations," *AIAA Journal*, Vol. 48, No. 11, 2010, pp. 2564–2575.

[40]Leung, T. and Zingg, D. W., "Aerodynamic Shape Optimization of Wings Using a Parallel Newton-Krylov Approach," *AIAA Journal*, Vol. 50, No. 3, 2012, pp. 540–550.

[41]Leung, T. M. and Zingg, D. W., "Design of Low-Sweep Wings for Maximum Range," *29th AIAA Applied Aerodynamics Conference*, AIAA-2011-3178, Honolulu, HI, June 2011.

[42]Gagnon, H. and Zingg, D. W., "High-fidelity Aerodynamic Shape Optimization of Unconventional Aircraft through Axial Deformation," *52nd Aerospace Sciences Meeting*, AIAA-2014-0908, National Harbor, MD, January 2014.

[43]Zhang, Z. J., Khosravi, S., and Zingg, D. W., "High-Fidelity Aerostructural Optimization with Integrated Geometry Parameterization and Mesh Movement," *56th AIAA/ASCE/AHS/ASC Structures, Structural Dynamics, and Materials Conference*, AIAA-2015-1132, Kissimmee, FL, January 2015.

[44]Khosravi, S. and Zingg, D. W., "A Numerical Optimization Study on Winglets," *15th AIAA/ISSMO Multidisciplinary Analysis and Optimization Conference*, AIAA-2014-2173, Atlanta, GA, June 2014.